Corrosion Science 53 (2011) 2988–2993

Contents lists available at ScienceDirect

Corrosion Science

journal homepage: www.elsevier.com/locate/corsci

Corrosion behaviour of sputter-deposited Mg–Zr alloys in a borate buffer solution

A.A. El-Moneim [a,*], E. Akiyama [b], K.M. Ismail [c], K. Hashimoto [d]

[a] Materials Science and Engineering Department, Egypt–Japan University of Science and Technology, New Borg Al Arab, Alexandria, Egypt
[b] Structural Metals Centre, National Institute for Materials Science, Tsukuba 305-0047, Japan
[c] Department of Chemistry, Faculty of Science, University of Cairo, Giza, Egypt
[d] Tohoku Institute of Technology, Sendai 982-8588, Japan

ARTICLE INFO

Article history:
Received 25 February 2011
Accepted 12 May 2011
Available online 18 May 2011

Keywords:
A. Magnesium
A. Zirconium
A. Sputtered films
B. XPS
B. XRD
C. Passive film

ABSTRACT

Corrosion behaviour of sputter-deposited Mg–Zr alloys was examined in a borate buffer solution of pH 8.7. XRD measurements showed that the alloys were supersaturated with Zr. The addition of 29 at.% Zr or more was very effective in increasing the corrosion resistance of Mg by more than four orders of magnitude. XPS analysis of spontaneously formed passive films revealed that the passive film consisted of double oxyhydroxide composed of enriched tetravalent Zr and divalent Mg cations. The enrichment of Zr cations in the passive film is responsible for the enhanced corrosion resistance of Mg–Zr alloys.

1. Introduction

The application of Mg and its alloys in various engineering fields has increased steadily in recent years because Mg alloys exhibit an attractive combination of low density and high ratio of strength to weight. Due to their remarkable properties, the corrosion performance of Mg alloys has attracted considerable attention in recent years [1–6]. However, these alloys are very reactive in nature, and the surface film formed on the alloys naturally cannot provide enough protection [1,2]. Their insufficient corrosion resistance has been a serious limitation to wider application of Mg alloys in practice.

In general, alloying with valve metals, such as Zr, Ti and Ta, is an effective mean for improving corrosion resistance and mechanical properties of many metals and alloys. For instance, addition of small amount of Zr, which is one of the corrosion resistant metals, to Mg has shown an exceptional grain-refining effect, and the Zr addition is an effective approach to improve the mechanical properties of magnesium-based alloys [7–9]. However, due to the limited solubility of Zr in Mg (ca. 1 at.%), the alloys formed by conventional casting techniques, such as chemical reduction and melting techniques, usually contain a large number of undissolved Zr precipitates with dimensions over 10 μm. The Zr precipitates generate micro-galvanic cells with the alloy matrix and adversely affect on their corrosion resistance [7–9].

Over the past couple of decades, sputter-deposition method has gained a great importance in improving corrosion resistance as well as reducing the adverse effects of alloying elements owing to the formation of a homogeneous single solid-solution phase even when the boiling point of one component is higher than the melting points of the rest of components and/or when one component is immiscible with another in the liquid state [10–17]. The homogeneous single-phase nature leads to the formation of a uniform passive film composed mainly of passivating elements or solid-solution-mixed oxide or oxyhydroxide which is able to separate the bulk of the alloy from an aggressive environment, and hence is responsible for high corrosion resistance [7–16,18–24]. Even if amorphous single-phase alloys are not formed, the alloys thus prepared are always composed of microcrystals with fine grains and often behave similarly to solid solution alloys [25–27].

By utilising the advantage of sputter-deposition technique, an attempt has been carried out in the present investigation to improve the corrosion resistance of Mg by alloying with Zr. To the best of our knowledge no information about the electrochemical behaviour and corrosion stability of sputter-deposited Mg–Zr alloys has been reported in the literature.

In this work, the electrochemical behaviour and corrosion stability of newly developed sputter-deposited Mg–Zr alloys over a wide composition range have been investigated in a borate buffer solution of pH 8.7. Special attention was directed to examine the effect of passive film composition and structure on the corrosion stability of the alloys.

* Corresponding author. Tel.: +20 181229081; fax: +20 34599520.
E-mail address: ahmed.abdelmoneim@ejust.edu.eg (A.A. El-Moneim).

0010-938X/$ - see front matter © 2011 Elsevier Ltd. All rights reserved.
doi:10.1016/j.corsci.2011.05.043

2. Experimental

The Mg–Zr alloys were prepared using a D.C. magnetron sputtering technique on glass substrates [28,29]. The glass substrates were rinsed by immersion in water containing a commercial detergent at 75 °C. Water cooled three substrates were installed in the sputtering chamber facing the target. For the sake of homogeneity of the sputter-deposits the substrates were revolved around the central axis of the chamber, so that the substrates pass right above the target, in addition to the revolution of the substrates themselves around their own axes. After pre-sputtering of the target for 30 min, the sputtering of the substrate was conducted at 4–9×10^{-4} Torr of argon gas. The composition of sputter-deposits was controlled by changing the number of daughter Mg plates on the mother Zr disk target.

The alloy compositions were determined by electron probe microanalysis (Shimadzu EPMA-C I). The structure of sputter-deposited alloys was identified by X-ray diffraction with Cu K_α radiation at θ-2θ mode. The grain size was estimated by using Scherrer's equation [30].

Gravimetric and electrochemical measurements were conducted in a naturally aerated borate buffer solution (0.075 M $Na_2B_4O_7$ + 0.3 M H_3BO_3) of pH 8.7 as mild environment to understand the effect of passive film composition and structure on the corrosion behaviour of Mg–Zr alloys.

Prior to the gravimetric and electrochemical experiments the samples were mechanically polished with diamond spray down to 0.25 μm and were cleaned in acetone. Potentiodynamic polarisation was carried out after the open-circuit potential of the specimen in the test solution became steady. A potential sweep rate was 1 mV s^{-1}. The counter electrode was a large-area Pt wire. Saturated calomel electrode (SCE) was used as a reference electrode.

X-ray photoelectron spectra were measured using a Shimadzu-ESCA 850 photoelectron spectrometer with Mg K_α excitation for surface analysis. Binding energies of electrons were calibrated using the method described elsewhere [31–33]. The binding energies of Au $4f_{7/2}$ and $4f_{5/2}$ electrons of gold metal and Cu $2p_{3/2}$ and $2p_{1/2}$ electrons of Cu metal were taken as 84.07, 87.74, 952.53 and 952.35 eV, respectively, and the kinetic energy of the Cu $L_3M_{4,5}$ Auger electrons of Cu metal was taken as 918.65 eV. The binding energies at the peaks observed in photoelectron spectra were further corrected by taking the binding energy of C 1s as 285.0 eV when the specimen showed charging effect. The composition and thickness of the surface film were quantitatively determined by a previously proposed method using integrated intensities of X-ray photoelectron spectra [34,35]. The sensitivity factor of Mg $KL_{2,3}L_{2,3}$ Auger electrons against the O 1s photoelectrons used was 3.71 [36]. The photoionization cross-section of Zr 3d electrons relative to that of O ls electrons used was 2.561 [37]. For angle-resolved XPS, the angle between the specimen surface and the direction of photoelectron to the detector (take-off angle) was changed by using tilted specimen stages. Other XPS measurements were carried out at fixed take-off angle of 90°.

3. Results and discussion

Hereafter, all sputter-deposited Mg–Zr alloys with various compositions were denoted in atomic percentage. Mg–Zr alloys containing from 6 to 81 at.% Zr were prepared and their corrosion behaviour was studied in a naturally aerated borate buffer solution (0.075 M $Na_2B_4O_7$ + 0.3 M H_3BO_3) of pH 8.7 at 30 °C.

3.1. Structure of Mg–Zr alloys

Fig. 1 shows XRD patterns for bulk Mg metal and sputter-deposited Mg–Zr alloys with different Zr content. X-ray diffraction patterns show the formation of the alloys with the hexagonal close packed structure. The intense 0 0 2 reflection of alloys suggests the presence of the 0 0 1 preferred orientation in the Mg–Zr alloys, in contrast to polycrystalline magnesium. Sputter deposition is known to form often amorphous alloys. However, because both Mg and Zr crystallize in the same hexagonal close packed structure, amorphous Mg–Zr alloys are not formed by sputter deposition. In this connection, the 0 0 2 lattice spacing decreases with the Zr content of the alloys as shown in Fig. 2. This fact indicates that sputter deposition led to formation of the solid solution alloys of a single phase, far exceeding the equilibrium solubility limit of zirconium in magnesium. The grain size was estimated by using Scherrer's equation [30] from the full width at half maximum of the 0 0 2 reflection. The estimated grain size, also shown in Fig. 2, decreases with increase in Zr content. The continuous change of estimated grain size of the Mg–Zr alloys also supports the formation of the solid solution alloys of a single phase.

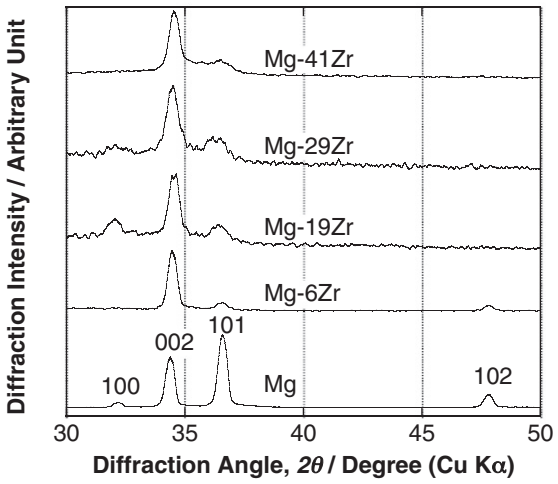

Fig. 1. XRD patterns of bulk Mg metal and sputter-deposited Mg–Zr alloys with varied Zr content.

Thus, although it is commonly known that the solubility of Zr in Mg is very limited (about 1 at.%), sputter deposition makes it possible to supersaturate Zr in Mg [10]. The alloys consisted of single-phase solid solution, and hence it is interesting to clarify the beneficial effect of alloying Zr on the passivity and corrosion stability of the single phase Mg–Zr alloys.

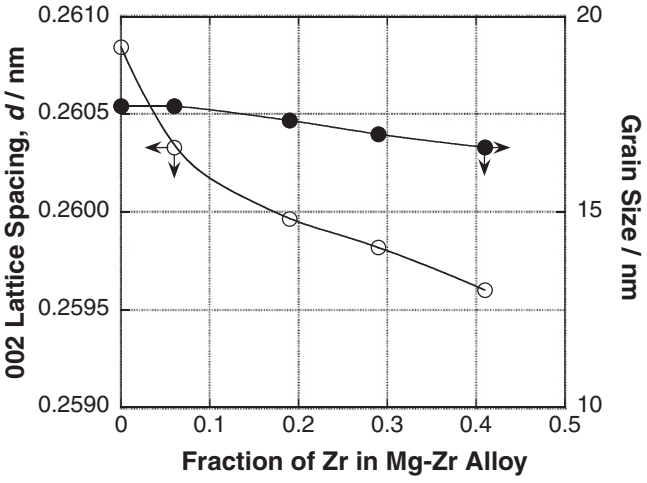

Fig. 2. 0 0 2 lattice spacing and estimated grain size of bulk Mg metal and sputter-deposited Mg–Zr alloys with varied Zr content.

3.2. Corrosion rates of sputter-deposited Mg–Zr alloys

Fig. 3 presents the corrosion rates of sputter-deposited Zr metal and Mg–Zr alloys. The corrosion rate of bulk Mg metal is also presented for comparison. The corrosion rates of sputter-deposited Mg–Zr alloys estimated from the measured loss in the alloys weight after immersion for 1 week in borate solution of pH 8.7 at 30 °C. Due to hydrogen gas evolution during dissolution of Mg metal and its subsequent physico-mechanical effect on the corrosion behaviour of Mg metal, the corrosion rate estimated after about 7 h of immersion in borate solution. The corrosion rate of pure Mg was 0.25 mm y^{-1}. In contrast, the corrosion rate of the sputter-deposited Mg–Zr alloys decreased almost exponentially with the increase in the Zr content up to 29 at.%, and then remained at about 0.35×10^{-4} mm y^{-1} almost unchanged with further increase in Zr content.

The corrosion rate of the Mg–Zr alloys containing 29 at.% Zr or more was about four orders of magnitude lower than that of the bulk Mg metal. Therefore, the formation of single-phase solid solution alloys seems to be responsible for the improvement in the corrosion resistance of the alloys.

3.3. Open circuit potential measurements

Fig. 4 shows open circuit potentials of bulk Mg metal, sputter-deposited Zr metal and Mg–Zr alloys in a borate buffer solution of pH 8.7. For bulk Mg metal, the open circuit potential was about −1.8 V (SCE). On the other hand, the open circuit potential of sputter-deposited Zr was nobler at about −0.4 V (SCE). In general, the open circuit potential of the alloys shifts toward noble direction with increase in Zr content. The open circuit potentials of the Mg–Zr alloys containing 41 at.% of Zr or more, whose corrosion rates were similar to that of pure Zr, were comparable to or higher than that of sputter-deposited Zr.

The open circuit potential of Mg–Zr alloys containing 19 at.% Zr or more tended to shift towards noble direction with immersion time. This behaviour can be attributed to the initial selective dissolution of Mg followed by passivation of Zr-enriched surface as will be discussed using XPS data later. Sputter-deposited Zr and samples containing ⩾55 at.% Zr reached steady potential within very short time of immersion in the borate buffer solution.

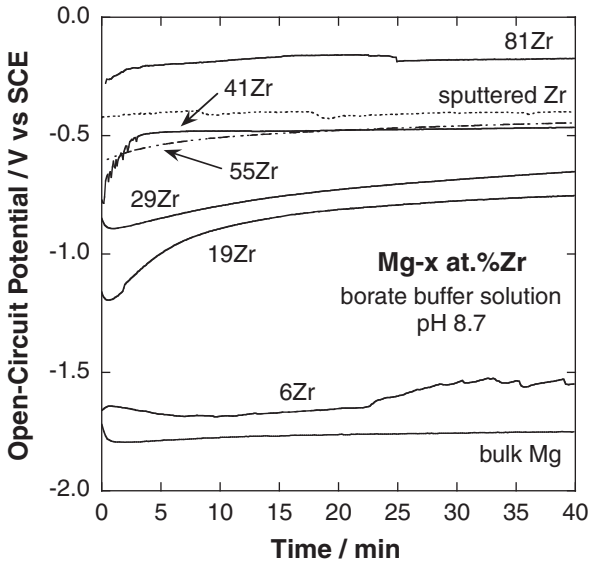

Fig. 4. Change in open-circuit potentials of sputter-deposited Mg–Zr alloys, bulk Mg and sputter-deposited Zr with immersion time in a borate buffer solution of pH 8.7 at 30 °C.

3.4. Potentiodynamic polarisation

Fig. 5 shows potentiodynamic polarisation curves of sputter-deposited Mg–Zr alloys and bulk Mg metal measured after immersion in a borate buffer solution for 1 h. Mg metal dissolves actively with very high corrosion current. The alloying addition of Zr significantly suppressed the active dissolution of Mg and the Zr-containing alloys were spontaneously passivated. The corrosion current density decreased significantly with increasing Zr content up to 29 at.%, and they stayed at roughly the same level of 1 to 4×10^{-4} A cm^{-2} with further increase in Zr content. These

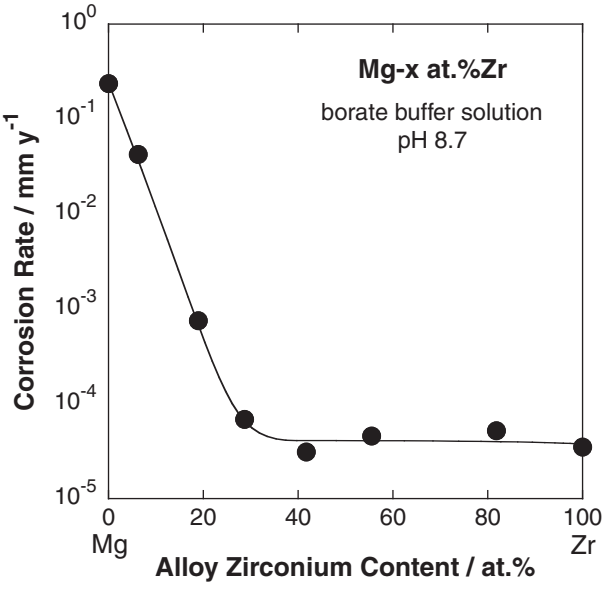

Fig. 3. Change in corrosion rate of sputter-deposited Mg–Zr alloys with Zr content in a borate buffer solution of pH 8.7 at 30 °C for 1 week. Corrosion rate of bulk Mg metal obtained after about 7 h of immersion in the solution is also shown for comparison.

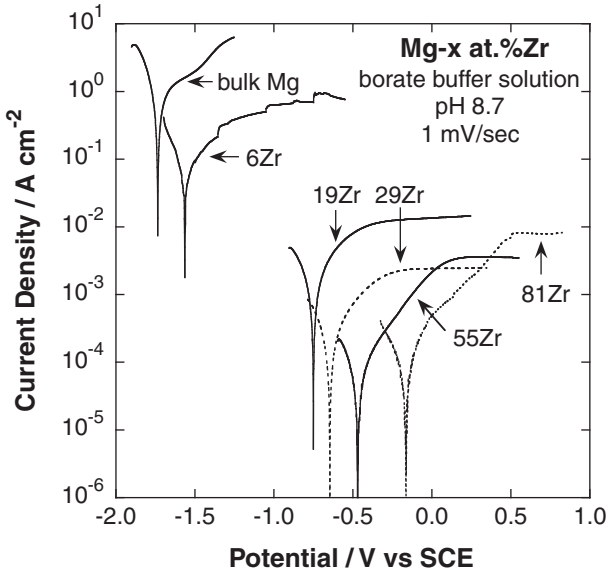

Fig. 5. Potentiodynamic polarisation curves of sputter-deposited Mg–Zr alloys and bulk Mg in a borate buffer solution of pH 8.7 at 30 °C.

observations are in agreements with the results of corrosion rate presented in Fig. 3, indicative of the barrier nature of passive film formed on Mg–Zr alloys.

Thus, superior corrosion resistance and passivation ability of Mg–Zr alloys compared to that of Mg was detected in the borate solution. This is mainly attributed to the beneficial effect of the alloying component, Zr, which is mixed with Mg in a homogeneous phase.

3.5. X-ray photoelectron spectroscopy (XPS) investigation

The presence of C, B, O, Mg and Zr peaks was identified in the X-ray photoelectron spectra of the surface of the alloys after immersion in the borate buffer solution. The contaminant carbon peak presumably originated from the residuals of the vapours of the oil pumps [3,23] was very small.

The X-ray photoelectron spectra from the alloy constituents indicated the presence of oxidised species coming from the surface film and metallic species coming from the underlying alloy surface beneath the surface film. The measured spectra of Zr $3d_{5/2}$ and Mg $2p_{3/2}$ were separated into Zr^{4+}, Zr^0, Mg^{2+} and Mg^0 spectra, respectively. An example spectrum of the Mg $2p_{3/2}$ is given in Fig. 6, which showed a single peak corresponding to Mg^{2+} state at about 51.3 eV and another peak corresponding to Mg^0, the metallic state, at 49.3 eV. The spectrum shown in Fig. 6 was measured for bulk Mg after mechanical polishing. The Zr $3d_{5/2}$ spectrum was composed of two peaks. The high binding energy peak appeared at 182.4 eV was corresponding to Zr^{4+} state. Another peak corresponding to Zr^0 for the metallic state was located at 178.8 eV. The composition of the surface film and the underlying alloy surface were determined quantitatively by integrating the intensities of the spectra for each species using the method described elsewhere [20–23,34,35].

Fig. 7 shows the change in the cationic fraction in the surface film and the atomic fraction in the underlying alloy surface as a function of alloy Zr content of Mg–Zr alloys, before, i.e. after mechanical polishing in cyclohexane, and after immersion in a borate buffer solution of pH 8.7 at 30 °C for 1 h. The XPS results reveal that the compositions of the air-formed film formed after the mechanical polishing and the underlying alloy surface beneath the air-formed film are similar to that of the bulk alloy composition. On the other hand, it is noteworthy that the surface films were enriched in Zr cations by the immersion, associated with enrichment of Mg at the underlying alloy surface. These

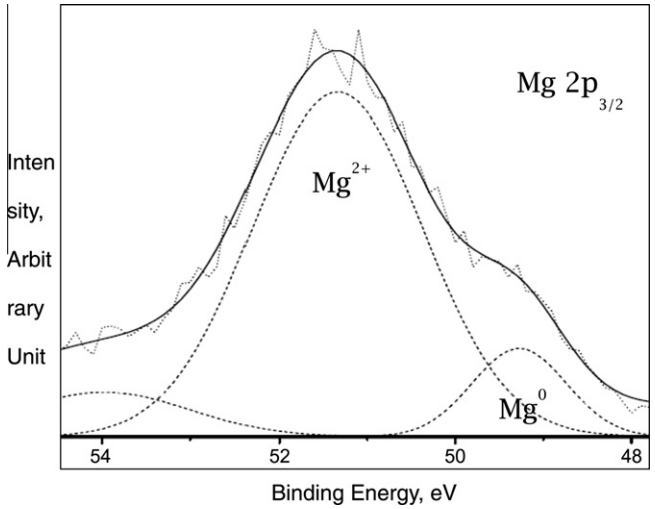

Fig. 6. A typical Mg $2p_{3/2}$ spectrum measured using XPS. The spectrum is deconvoluted into spectra for Mg in metallic state and oxidised state, Mg^{2+}. The spectrum is of as-polished bulk Mg.

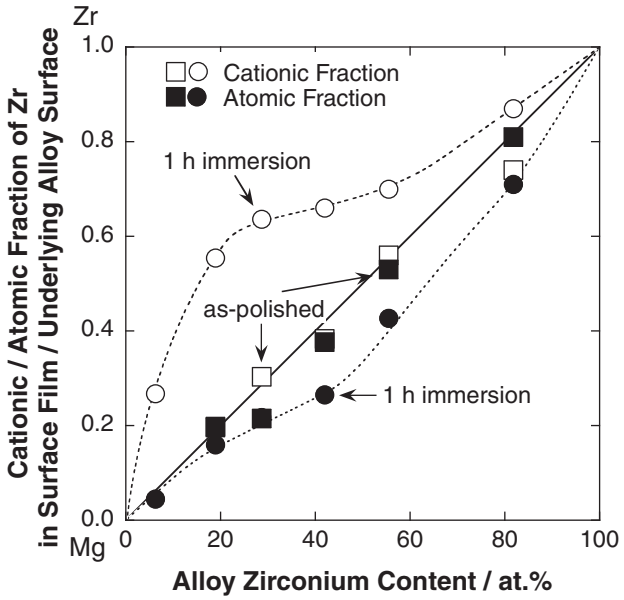

Fig. 7. Dependence of cationic and atomic compositions of surface film and underlying alloy surface, respectively, on alloy Zr content of sputter-deposited Mg–Zr alloys. The surface compositions were obtained using XPS analyses after mechanical polishing in cyclohexane and immersion in a borate buffer solution of pH 8.7 at 30 °C for 1 h.

composition changes by immersion are presumably caused by both preferential dissolution of Mg from the surface film and preferential oxidation of Zr at the underlying alloy surface. The improved resistance of Mg–Zr alloys is most probably due to the enrichment of passivating elements, Zr, in the surface film. The cationic fraction of Zr higher than 0.6 corresponds to the significantly decreased corrosion rate which is almost 4 orders of magnitude lower than that of bulk Mg (Fig. 3).

The presence of the oxygen peak (O 1s) was composed of two overlapping peaks corresponding to OM and OH oxygen peaks. The OM oxygen corresponds to O^{2-} anions in the oxide of the surface film. The other oxygen peak originated from OH^- ions and H_2O presenting in the oxyhydroxide and hydrated layer of the surface film. Fig. 8 shows the variation in the ratio of $[O^{2-}]$ and $[OH^- + H_2O]$ to [cations] in the surface films as a function of alloy Zr content after immersion in the borate solution for 1 h. The ratio of $[OH^- + H_2O]$/[cations] in the surface film of pure Mg was about 10 times higher than $[O^{2-}]$/[cation]. The ratio of $[OH^- + H_2O]$/[cation] was always higher than that of $[O^{2-}]$/[cation] for all the examined Mg–Zr alloys. Meanwhile, a significant decrease in the ratio of $[OH^- + H_2O]$/[cation] along with an increase in $[O^{2-}]$/[cation] is noticed with the increase in alloy Zr content. The increase in $[O^{2-}]$/[cation] suggests the development of surface film in which oxo-bridging of constituent cations are promoted and its protective ability is improved rather than the film with higher OH^- ratio.

The transient behaviour in the compositions of surface film and underlying alloy surface just beneath the surface film for Mg-29Zr and Mg-41Zr alloys with immersion time is shown in Fig. 9. The results reveal that the immersion for only 1 min leads to the obvious enrichment of Zr cations in the surface film and the slight depletion of Zr in the underlying alloy surface. The cationic and atomic fractions of Zr in both passive film and underlying alloy surface did not change significantly with the prolonged immersion time. The increase in the open circuit potential in relatively short time of immersion shown in Fig. 3 is probably correspondent with the enrichment of Zr cations in the surface film.

For further information about the nature of the passive film formed on the Mg–Zr alloys and for characterising the in-depth

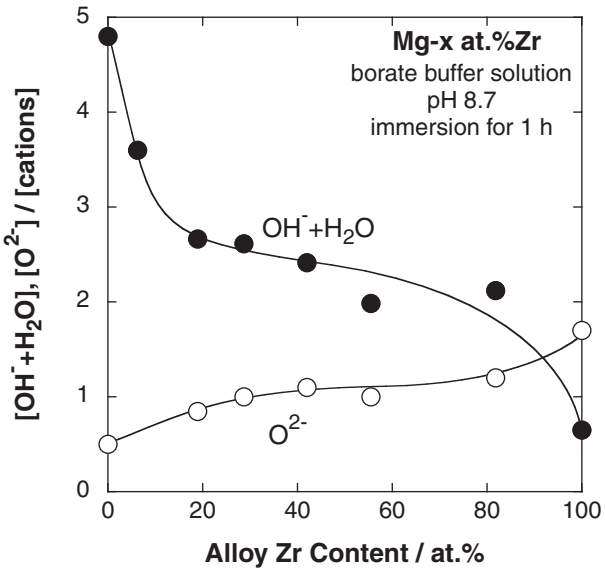

Fig. 8. Ratios of concentration of oxygen species to concentration of cationic constituents in surface films formed on Mg–Zr alloys as a function of alloy Zr content. The Mg–Zr alloys were immersed in a borate buffer solution of pH 8.7 at 30 °C for 1 h. The oxygen-species ratios of bulk Mg and sputter-deposited Zr are also shown for comparison.

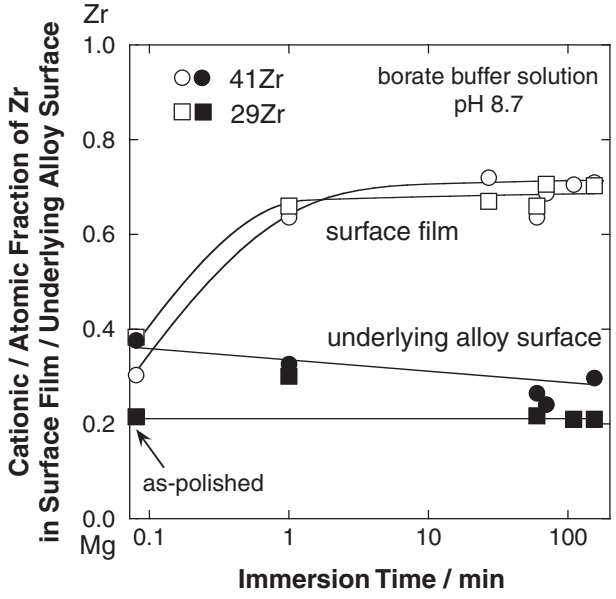

Fig. 9. Change in cationic and atomic fractions of Zr in surface film and underlying alloy surface, respectively, with time of immersion of Mg–Zr alloys in a borate buffer solution of pH 8.7 at 30 °C.

distribution of constituents in the surface film and the underlying alloy surface, angle-resolved XPS measurements were performed. In the experiments, the surface sensitivity was varied by changing the angle of detection of photoelectron from the specimen surface. At lower angles of detection with respect to the surface (take-off angle), the signal from the species located in the external part is more enhanced than at higher take-off angles.

Fig. 10(a) and (b) show the take-off angle dependence of the compositions of surface film and underlying alloy surface, respectively, of Mg-29Zr alloy before and after immersion in the borate buffer solution for 1 min and 155 min. Zr cations showed clear concentration gradient in the surface film and that changed with immersion time, suggesting that the in-depth distribution of cations changed with dissolution. In the air-formed film before immersion, Zr cations were slightly depleted in the exterior part. Zr cations, by contrary, were significantly concentrated especially in the exterior part of the passive film after open-circuit immersion associated with depletion of Zr in at the underlying alloy surface. Extension of the immersion time led to an increase of the measured cationic fraction of Zr at higher take-off angle. This result suggests that the enrichment of Zr in the interior of the passive film progressed with immersion time. It seems reasonable that the enrichment of Zr in passive film is of significance to the corrosion resistance of the Mg–Zr alloys in the borate buffer solution.

Another interesting feature of the structure of the surface film formed on Mg–Zr alloys after immersion in the borate buffer solution is the electronic interaction between Mg and Zr cations. Fig. 11 shows the change in the binding energies of core electrons of Mg $2p_{3/2}$ (Fig. 11(a)) and Zr $3d_{5/2}$ (Fig. 11(b)) as a function of cationic fraction of Zr in the surface film. In the figure the data of the

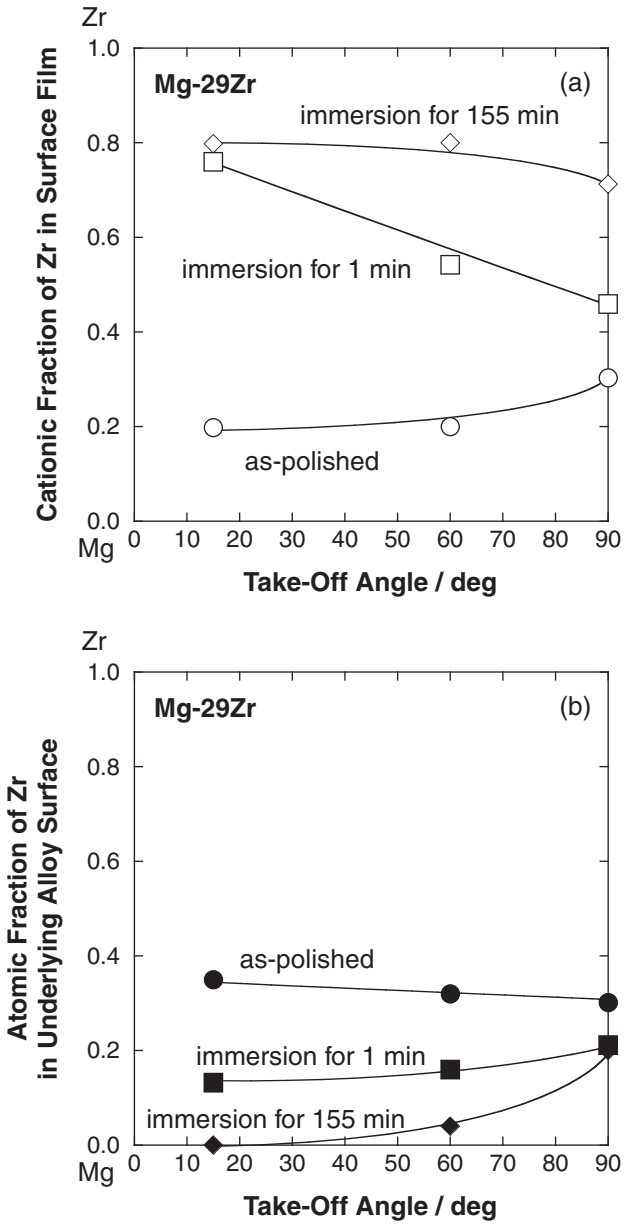

Fig. 10. Change in cationic fraction of Zr in surface film (a) and atomic fraction of Zr in underlying alloy surface (b) with take-off angle of photo electron for Mg-29Zr alloy after mechanical polishing, immersion in a borate buffer solution for 1 and 155 min.

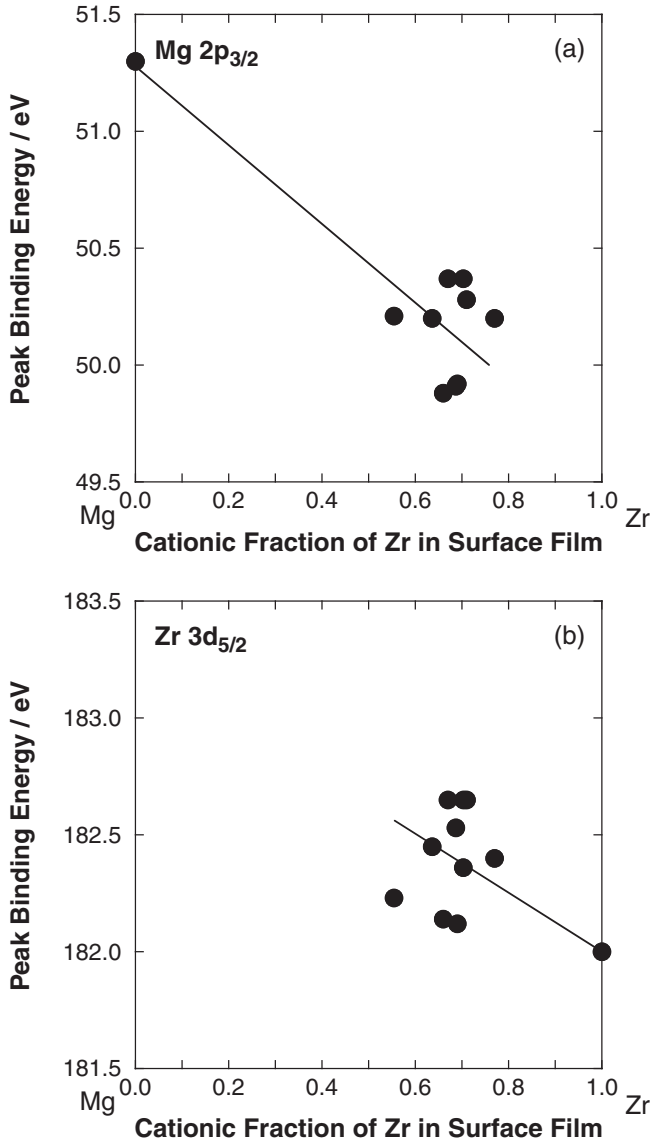

Fig. 11. Peak binding energies of Mg $2p_{3/2}$ (a) and Zr $3d_{5/2}$ (b) core electrons corresponding to Mg^{2+} and Zr^{4+}, respectively, in surface films formed by immersion with varied time in a borate buffer solution of pH 8.7. The peak binding energies are plotted as a function of cationic fraction of Zr in surface films.

surface films formed by different immersion times in the solution are shown together. The peak binding energy of Mg $2p_{3/2}$ electrons decreased with increasing Zr^{4+} content, while that of Zr $3d_{5/2}$ electrons increased with increasing Mg^{2+} content in the surface film. This fact indicates that charge transfer occurs from Zr^{4+} to Mg^{2+} in the passive film, signifying that Mg and Zr cations are located in very close proximity in the film. Consequently, the films formed on Mg–Zr alloys after immersions are not composed of simple mixture of Zr oxyhydroxide and Mg oxyhydroxide, but rather double oxyhydroxide enriched with Zr. This double oxyhydroxide film formed on the single phase Mg–Zr alloys seems to be responsible for their improved corrosion resistance.

4. Conclusions

The Mg–Zr alloys prepared by sputter-deposition method had crystalline structure with solid solution supersaturated with Zr. The addition of Zr reduced the dissolution rate and improves its passivation ability. The corrosion rate of sputter-deposited Mg–Zr alloys decreased almost exponentially with the increase of Zr content. Significant corrosion resistance similar to sputter-deposited Zr is obtained when Zr content was 29 at.% or more. The superior corrosion resistance and stability of the sputter-deposited Mg–Zr alloys compared to that of Mg is attributable to the formation of barrier–type surface film of Zr–Mg double oxyhydroxide enriched with Zr cations.

References

[1] G.L. Makar, J. Kruger, In. Mater. Rev. 38 (1993) 138–153.
[2] G.L. Song, A. Atrens, Adv. Eng. Mater. 1 (1999) 11–33.
[3] K.M. Ismail, S. Virtanen, Electrochem. Solid-State Lett. 10 (2007) C9–C11.
[4] Z. Chen, M. Zhang, W. Han, X. Wang, D. Tang, J. Alloys Compounds 459 (2008) 209–214.
[5] M.C. Turhan, R. Lynch, M.S. Killian, S. Virtanen, Electrochim. Acta 55 (2009) 250–257.
[6] R. Pinto, M.G.S. Ferreira, M.J. Carmezim, M.F. Montemor, Electrochim. Acta 55 (2010) 2482–2489.
[7] G. Song, D. StJohn, J. Light Met. 2 (2002) 1–16.
[8] Y. Tamura, N. Kono, T. Motegi, E. Sato, J. Jpn. Inst. Light Met. 47 (1997) 697–705.
[9] Y. Tamura, N. Kono, T. Motegi, E. Sato, J. Jpn. Inst. Light Met. 48 (1998) 185–189.
[10] E. Juzeliunas, A. Griguceviciene, K. Leinartas, R. Juskenas, Electrochem. Commun. 6 (2004) 678–682.
[11] G.S. Frankel, J.O. Dukovic, B.M. Rush, V. Brusic, C.V. Jahnes, J. Electrochem. Soc. 139 (1992) 2196–2201.
[12] G.S. Frankel, J.R. Scully, C.V. Jahnes, J. Electrochem. Soc. 143 (1996) 1834–1840.
[13] K. Hashimoto, J.H. Kim, P.Y. Park, E. Akiyama, H. Habazaki, A. Kawashima, K. Asami, Mater. Sci. Forum 185–188 (1995) 789–798.
[14] R. Hubler, Surf. Coat. Technol. 116–119 (1999) 1116–1122.
[15] J.H. Kim, P.Y. Park, E. Akiyama, H. Habazaki, A. Kawashima, K. Asami, K. Hashimoto, Corros. Sci. 33 (1992) 1507–1518.
[16] J.H. Kim, P.Y. Park, E. Akiyama, H. Habazaki, A. Kawashima, K. Asami, K. Hashimoto, Corros. Sci. 36 (1994) 511–523.
[17] K. Hashimoto, N. Kumagai, H. Yoshioka, J.H. Kim, E. Akiyama, H. Habazaki, S. Mrowec, A. Kawashima, K. Asami, Corros. Sci. 35 (1993) 363–370.
[18] A.A. El-Moneim, B.P. Zhang, E. Akiyama, H. Habazaki, A. Kawashima, K. Asami, K.K. Hashimoto, Corros. Sci. 39 (1997) 305–320.
[19] A.A. El-Moneim, E. Akiyama, H. Habazaki, A. Kawashima, K. Asami, K.K. Hashimoto, Corros. Sci. 39 (1997) 1965–1979.
[20] A.A. El-Moneim, E. Akiyama, H. Habazaki, A. Kawashima, K. Asami, K. Hashimoto, Corros. Sci. 40 (1998) 235–250.
[21] A.A. El-Moneim, E. Akiyama, H. Habazaki, A. Kawashima, K. Asami, K. Hashimoto, Corros. Sci. 40 (1998) 1491–1512.
[22] A.A. El-Moneim, E. Akiyama, H. Habazaki, A. Kawashima, K. Asami, K. Hashimoto, Corros. Sci. 40 (1998) 1513–1531.
[23] K.M. Ismail, A.A. El-Moneim, W.A. Badawy, J. Electrochem. Soc. 148 (2001) C81–C87.
[24] K.M. Ismail, A.A. El-Moneim, W.A. Badawy, Electrochim. Acta 47 (2002) 2463–2472.
[25] P.Y. Park, E. Akiyama, H. Habazaki, A. Kawashima, K. Asami, K. Hashimoto, Corros. Sci. 38 (1996) 1649–1667.
[26] P.Y. Park, E. Akiyama, H. Habazaki, A. Kawashima, K. Asami, K. Hashimoto, Corros. Sci. 38 (1996) 1731–1750.
[27] P.Y. Park, E. Akiyama, A. Kawashima, K. Asami, K. Hashimoto, Corros. Sci. 38 (1996) 397–411.
[28] E. Akyiama, H. Habazaki, A. Kawashima, K. Asami, K. Hashimoto, Corros. Sci. 38 (1996) 279–292.
[29] J.H. Kim, E. Akyiama, H. Habazaki, A. Kawashima, K. Asami, K. Hashimoto, Corros. Sci. 36 (1994) 511–523.
[30] P. Scherrer, Nachr. Ges. Wiss. Gottingen, 26 September (1918) 98–100.
[31] K. Asami, J. Electron Spectrosc. Relat. Phenom. 9 (1984) 469–476.
[32] K. Asami, J. Electron Spectrosc. 9 (1976) 469–478.
[33] K. Asami, K. Hashimoto, Corros. Sci. 17 (1977) 559–570.
[34] K. Asami, K. Hashimoto, Corros. Sci. 24 (1983) 83–97.
[35] K. Asami, K. Hashimoto, S. Shimodaira, Corros. Sci. 17 (1977) 713–723.
[36] K. Asami, M.S. De SA, V. Ashworth, Proc. 6th European Symposium on Corrosion Inhibitors, Ann Univ. Ferra, N.S., Sez V, Suppl. No.8 (1985) 769–781.
[37] J.H. Scofield, J. Electron Spectrosc. 8 (1976) 129–137.